# SAS v5.0 Scientific Validation report (XMM-SOC-USR-TN-0003)

## Observation 0099280101 - Revolution 84 - Mkn421

M.Ehle[1], M.Guainazzi[1], C.Gabriel[1], M.Denby[2]

[1] *XMM-Newton Science Operation Center, VILSPA, ESA, Apartado 50727, E-28080 Madrid, Spain*
[2] *XMM-Newton Science Survey Center, Department of Physics & Astronomy, University of Leicester, Leicester LE1 7RH, UK*

26 January 2001

We report the results of the scientific validation of the XMM-Newton Science Analysis System (SAS) version 5.0 (SASv5 hereinafter), performed on the data of observation nr.**0099280101**. These data belong to the XMM-Newton Performance Verification (PV) phase. They are free from data rights.

The reader is referred to the following URL: `http://xmm.vilspa.esa.es/public/xmm_sas_sv_top.html` for general information about the scope and the procedures of the SAS science validation, and for links to the available documentation on the SAS and the XMM-Newton data format.

# 1 Purpose of the observation and instrument modes

XMM-Newton observed the region containing the Active Galactic Nucleus Mkn 421 ($\alpha_{2000}$=$11^h04^m27^s.0$, $\delta_{2000}$=+38°12'32".0) on May 25 2000, between 11:04:27 and 21:45:33 UTC (revolution number 84). Brinkmann et al. (2001) have published preliminary scientific results of this observation.

The purpose of including this observation in the SAS science validation process was originally to:

- check the SAS scientific product generation functionality for p-n data in `TIMING` mode
- verify the accuracy of the continuum spectral fitting in the RGS.

The instrument modes used in this observation are listed in Tab. 1. The CCD4 chain of RGS2 failed in revolution 26, and is therefore not included in the data.

| Instrument | Exposure | Mode | Filter | Processed by PPS? |
|---|---|---|---|---|
| MOS1 | 3 | Fast Uncompress | Medium | Y |
| MOS1 | 4 | Small Window Free Running | Medium | N |
| MOS1 | 16 | Full Frame | CalClosed | N |
| MOS2 | 6 | Small window free running | Medium | Y |
| MOS2 | 7 | Fast Uncompressed | Medium | N |
| MOS2 | 17 | Fast Uncompressed | CalClosed | N |
| p-n | 8 | Fast Timing | Thick | Y |
| p-n | 10 | Small window | Thick | N |
| p-n | 18 | Full Frame | CalClosed | N |
| RGS1 | 1 | HER+SES | | Y |
| RGS1 | 14 | HER+SES | | Y |
| RGS2 | 2 | HER+SES | | Y |
| RGS2 | 15 | HER+SES | | Y |
| OM | 9 | Image | Blocked | N |
| OM | 11 | Image | Blocked | N |
| OM | 12 | Image | Blocked | N |
| OM | 13 | Flat Field | Blocked | N |

Table 1: Operational modes used

# 2 Pipeline products

The reader is referred to Sect. 2 of Guainazzi et al. (2001a). In addition, some of the observations originally present in the ODF were not processed by the PPS (cf. Tab. 1). There are two main reasons for that:

- exposures with "non-science" filters (*e.g.*: EPIC `CalClosed`) are currently not processed by the PPS

- `odfingest` did not recognize some of the EPIC camera exposure filters in this specific observation. These filters were labeled as "unknown" in the summary file created by `odfingest`. This prevented the PPS from recognizing the corresponding exposures as valid scientific ones.

Finally, some CCD boundaries are missing in the RGS source spectrum plots.

## 3 Functional tests on p-n TIMING mode data

The p-n `TIMING` mode exposure was affected by "counting mode" This configuration occurs whenever the telemetry rate is too high for the science packets to be properly filled. In this case the events are "deviated" into an housekeeping counter and therefore lost from the point of view of the science telemetry. The frame counter keeps on running, while no science events are registered.

Although this condition does not prevent a user from extracting scientific products (indeed images, pseudo-images, spectra and light curves can be created via `evselect/xmmselect`), it makes the interpretation of the results difficult. We defer therefore the proper validation of the SAS p-n `TIMING` mode analysis to a future report.

Moreover, the user is reminded that the EPIC response generator in SASv5 works only if the spectra are extracted from data in `IMAGING` mode.

## 4 Quality of RGS continuum spectral fitting

Previous soft X-ray observations of Mkn 421 (Takahashi et al. 1996; Guainazzi et al. 1999; Fossati et al. 2000) showed that its spectrum is characterized by a noticeably low level of photoelectric absorption, well consistent with the contribution of the line-of-sight Galactic $N_H$ ($N_{H_{Gal}} = 1.5 \times 10^{20}$ cm$^{-2}$). The spectrum can be at first order approximated with a broken power-law. Although this might be an oversimplification of the true picture, this model provides an adequate fit to both the p-n and MOS data (Brinkmann et al. 2001). The 1st order spectra (Fig. 1) of

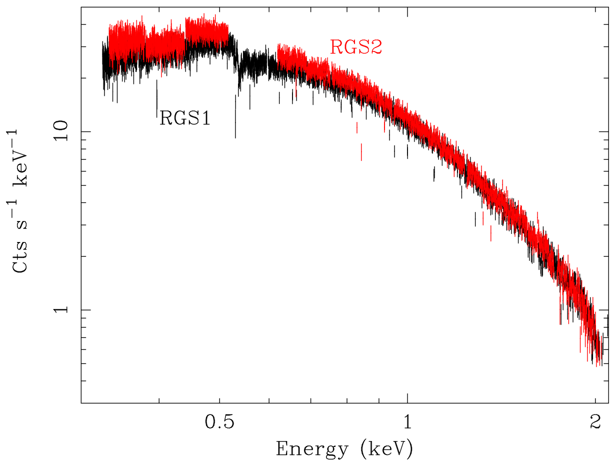


Figure 1: RGS1 (*black*) and RGS2 (*red*) spectra, as produced by the `rgsproc` SAS task with default input parameters. No rebinning is applied to the data points. Only the spectra corresponding to exposure 1 and 2 are shown

the two exposures in which each RGS observation is split have been simultaneously fit. A constant factor has been added to the model to account for the ≃16% flux difference between the two exposures. However, RGS1 and RGS2 spectra have been fit separately.

In Tab. 2 we compare the results obtained by Brinkmann et al. (2001) with the fits performed on the RGS1 PPS-produced spectra and on the spectra produced by running `rgsproc` on the ODF[1]. Response matrices have been generated with `rgsrmfgen`. This response generator is still in development and there are understood deficiencies. These include the response at wavelengths $\lesssim 9$ Å(*i.e.*: $E \gtrsim 1.4$ keV) and around the K-shell photoelectric threshold energy of O I ($E \simeq 0.55$ keV; Erd 2000); the efficiency of CCD2 in RGS2; and the relative efficiency of RGS1 compared

[1]A detailed description of the PPS pipeline and of the SAS `*proc` tasks can be found in Osborne (2000) and Gondoin (2000), respectively. The reader is also referred to the on-line SAS help pages

| | $\Gamma_1$ | $\Gamma_2$ | $E_{break}$ (keV) | 0.5–1.5 flux ($10^{-10}$ erg cm$^{-2}$ s$^{-1}$) | $\chi^2$/dof ($\chi^2_\nu$) |
|---|---|---|---|---|---|
| RGS1 | | | | | |
| Brinkmann et al. 2001 | $1.76 \pm 0.01$ | $1.94 \pm 0.01$ | $0.89^{+0.04}_{-0.03}$ | ... | (1.68) |
| PPS | $1.761^{+0.007}_{-0.006}$ | $2.24^{+0.08}_{-0.07}$ | $1.05 \pm 0.03$ | 2.68 | 10119.0/5148 (1.96) |
| `rgsproc` | $1.785 \pm 0.006$ | $2.03 \pm 0.05$ | $1.06^{+0.03}_{-0.02}$ | 2.70 | 12360.4/5826 (1.89) |
| RGS2 | | | | | |
| PPS | $1.803^{+0.007}_{-0.008}$ | $2.17 \pm 0.02$ | $0.819^{+0.015}_{-0.012}$ | 2.95 | 9002.9/4342 (2.07) |
| `rgsproc` | $1.865 \pm 0.007$ | $2.063 \pm 0.015$ | $0.816^{+0.018}_{-0.023}$ | 2.97 | 8296.2/4397 (1.89) |

Table 2: Best-fit parameters and results when a broken power-law model is applied to the RGS1 spectra of Mkn 421. The rows refers to the results of Brinkmann et al. (2001); to the fit applied to the spectra produced by the PPS, and by the `rgsproc` SAS pipeline

to RGS2. In the light of these features, the spectral fits presented below have been performed in the energy band below 1.4 keV only. A new version of the RGS response generator will be included in the SAS later this year.

In Fig. 2 the residuals (in terms of data/model ratio) against the best-fits are shown. The RGS1 (RGS2) 0.5–2 keV flux, corresponding to the best-fit model, is 3.3 (3.5)$\times 10^{-10}$ erg cm$^{-2}$ s$^{-1}$. It is consistent with the p-n value quoted by Brinkmann et al. [2001; $(2.9^{+0.5}_{-0.6}) \times 10^{-10}$ erg cm$^{-2}$ s$^{-1}$].

No significant difference exists between the spectra produced by the PPS and those produced with `rgsproc`. Nonetheless the statistics is so good, that even the small differences in the best-fit face values of the soft power-law branch spectral index, $\Gamma_1$ (2% on the RGS1 and 3% in the RGS2 for the softer branch of the power-law), are beyond the statistical uncertainties. The higher energy branch of the power-law is more poorly determined and likely to be somewhat affected by the residual uncertainties in the harder band of the response matrix. Moreover, the $\Gamma_1$ values in RGS1 are 3% flatter than in RGS2. This reflects in a 30% smaller break energy in the RGS2.

The residuals are within about $\pm 10\%$. The most critical area corresponds to the CCD2, whose effective area is lower by 10–15% than its neighbor CCDs (this effect is more markedly visible in RGS2). An absorption-like feature is visible in RGS1 CCD4 at $E \gtrsim 0.55$ keV. As mentioned above, all these features are consistent with the currently expected scientific quality of the calibrations available in the SAS calibration files (cf. Erd 2000).

The data show also a few "stray" outliners at a level $\lesssim 20\%$. They are due to a still unexplained error in the data processing. The origin of this feature is under investigation.

## Acknowledgments

The authors acknowledge useful discussions with D.Lumb, and comments by G.Branduardi-Raymond, C.Erd, W.Pietsch, J.Osborne, and J.W. van der Herder.

## References

W.Brinkmann, et al., 2001, A&A, 365, L162

C.Erd, 2000, XMM-CCF-REL-12, available at `http://xmm.vilspa.esa.es/docs/documents/CAL-SRN-0012-1-0.ps.gz`

G.Fossati, et al., 2000, MNRAS, in press (astro-ph/0005066)

P.Gondoin, 2000, *User's Guide of the XMM-Newton Science Analysis System*, available at `http://xmm.vilspa.esa.es/sas/xmmsas_20001215_0000/htmldoc/doc/userguide.ps.gz`

M.Guainazzi et al., 1999, A&A, 342, 124

M.Guainazzi et al., 2001a, XMM-SOC-USR-TN-0001 (*SAS v5.0 Scientific Validation report - Lockman Hole*), available at: `http://xmm.vilspa.esa.es/docs/documents/USR-TN-0001-1-0.ps.gz`

M.Guainazzi et al., 2001b, XMM-SOC-USR-TN-0002 (*SAS v5.0 Scientific Validation report - G21.5*), available at: `http://xmm.vilspa.esa.es/docs/documents/USR-TN-0002-1-2.ps.gz`

J.Osborne, 2000, SSC-LUX-SP-0004, available at `http://xmmssc-www.stare.le.ac.uk/pubdocs/SSC-LUX-SP-0004.ps.gz`

T.Takahashi, et al., 1996, ApJ, 470, L89

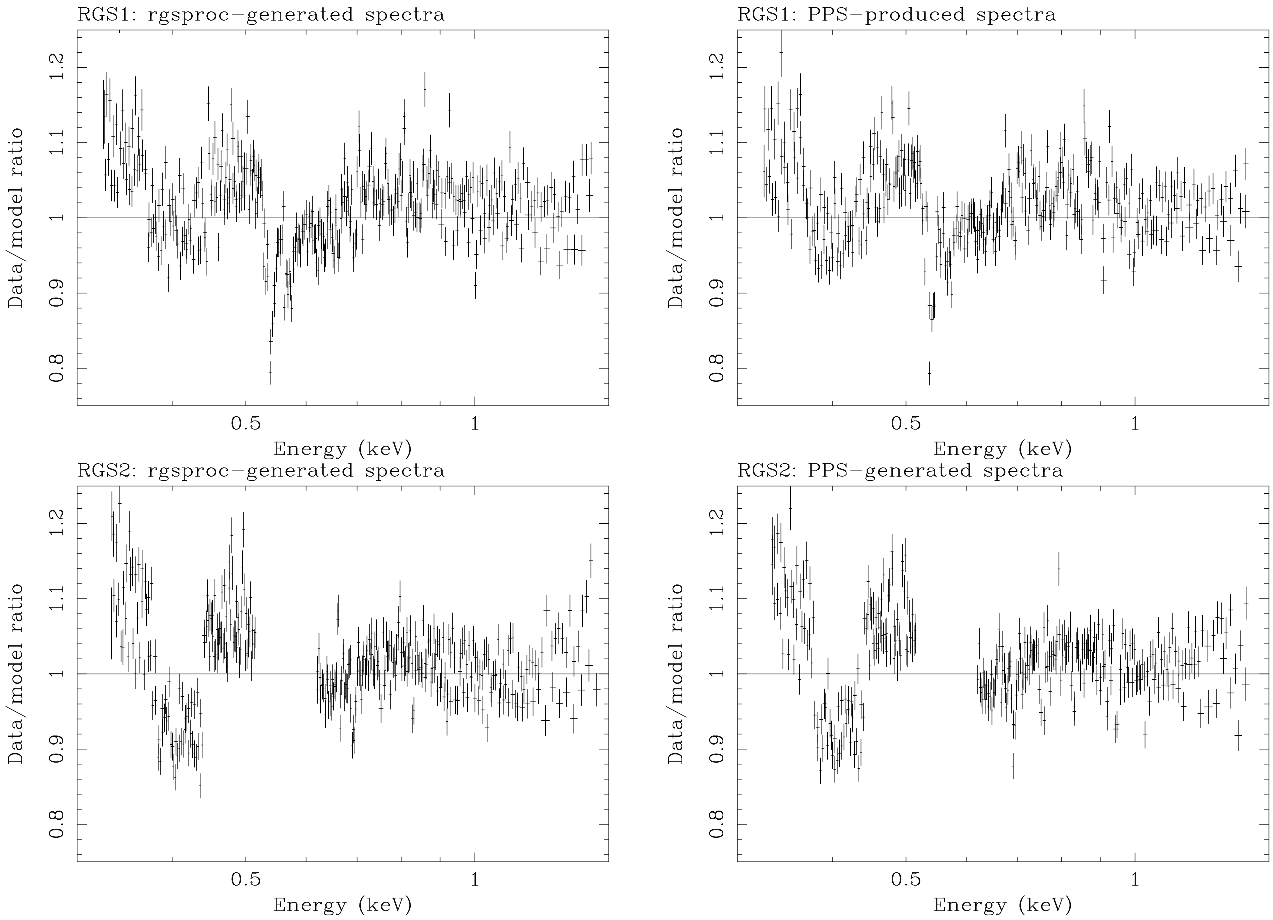


Figure 2: Residuals in data/model ratio (±25%) when a broken power-law model is applied to the Mkn 421 RGS spectra. *Upper left*: `rgsproc`-produced RGS1. *Upper right*: `rgsproc`-produced RGS2. *Lower left*: PPS-produced RGS1. *Lower right*: PPS-produced RGS2. Each data point corresponds to a S/N ratio >50